QUANTIZATION OF MAPPINGS AND OTHER SIMPLE CLASSICAL MODELS

M. V. Berry

H. H. Wills Physics Laboratory
Bristol BS8 1TL, England

INTRODUCTION

This article is a brief review of simple models exploring different aspects of the classical limit of quantum mechanics. More detailed treatments have either already been published[1] or are being prepared for publication. The reason for choosing simple models rather than accurate simulations of physical systems of current experimental interest is that such systems often lie in parameter ranges that do not correspond to well-defined semiclassical regimes.[2-4]

The different semiclassical regimes correspond to stationary and nonstationary states and to classical motion that may be either regular (integrable) or irregular (chaotic).[5] The case of stationary quantum states for regular underlying classical motion is now well understood:[6] classical orbits wind round tori in phase space, and energies for which the action integrals, $\oint \mathbf{p} \cdot d\mathbf{q}/2\pi$, around the irreducible cycles of a torus are equal to a half-integer multiple of $\hbar$ are asymptotic approximations to the eigenvalues of the Hamiltonian. The other regimes are not well understood. It is remarkable that they can be modeled by classical systems with just one coordinate, q, so that motion may be studied in the phase plane q, p.

An evolving state can be associated with a curve in the phase plane, at least until the curve gets very complicated. This association is explained in the next section, and its application and breakdown are illustrated for a generic system possessing both regular and irregular trajectories in the third section and, in the antepenultimate section, for a purely regular system. The penultimate section is devoted to the quantum eigenvalue structure of a purely chaotic system (Arnol'd's Cat[7]) and the final section reports a study of a similar system (Sinai's Billiard[7,18]), the coordinate space of which is two-dimensional.

We shall not discuss here other important aspects of semiclassical mechanics, such as matrix elements[4,14] and the nodal structure of eigenfunctions.[4,12,13]

ASSOCIATING WAVE FUNCTIONS WITH CURVES IN THE PHASE PLANE

Let $\mathcal{C}_0$ be a smooth curve in the phase plane q, p (FIGURE 1) representing a family of classical trajectories at time $t = 0$. Individual trajectories are points on $\mathcal{C}_0$ distributed uniformly in a (generalized "angle") variable θ. The associated approximate wave function, $\phi(q, 0)$, is a series of contributions,

$$\phi(q, 0) = \sum_i a_i(q) \exp [ib_i(q)], \tag{1}$$

from all points q, $p_i(q)$ lying on $\mathcal{C}_0$ with coordinate q (FIGURE 1).

0077-8923/80/0357-0183 $01.75/1 © 1980. NYAS

The amplitude $a_i(q)$ is obtained from the correspondence principle, according to which the probability densities a_i^2 of the different contributions are proportional to the densities of the projections onto q of the branches of $\mathcal{C}_0$. Therefore,

$$a_i^2(q)\mathrm{d}q = K^2\mathrm{d}\theta_i, \tag{2}$$

where K is a constant. The phase $b_i(q)$ is obtained from de Broglie's rule, according to which the contributions to ϕ are waves with wavelength $h/p_i(q)$, so that

$$b_i\left(q + \frac{h}{p_i(q)}\right) - b_i(q) \simeq \frac{h}{p_i(q)}\frac{\mathrm{d}b_i(q)}{\mathrm{d}q} = 2\pi. \tag{3}$$

Combining (2), (3), and (1) gives

$$\phi(q, 0) = K\sum_i \left|\frac{\mathrm{d}q}{\mathrm{d}\theta}\right|^{-1/2}_{(\theta=\theta_i(q))} \exp\left[i\int_{q_0}^{q}\frac{p_i(q')}{\hbar}\mathrm{d}q' - \delta_i\right]. \tag{4}$$

where q_0 is a constant and δ_i are phases that will not be discussed further here.

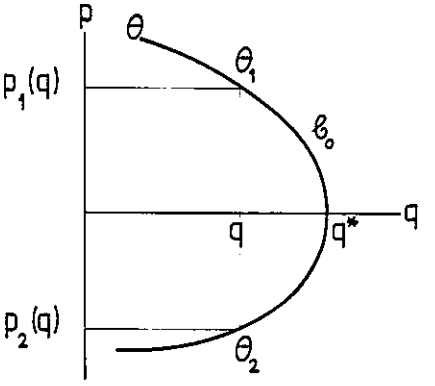

FIGURE 1. The curve $\mathcal{C}_0$, parameterized by "angle" variable θ, with momenta p_1 and p_2 contributing to the wave at q.

Inasmuch as a wave ϕ can be generated according to (4) from any curve $\mathcal{C}_0$, the association might seem arbitrary. In fact, it is not, because the association is preserved as the state changes. In time t, $\mathcal{C}_0$ evolves, by virtue of the classical motion of each of its points, into a new curve, $\mathcal{C}_t$, to which can be associated a wave $\phi(q, t)$ analogous to (4); using the WKB method of quantum mechanics,[8] or some other,[1] it can be shown that, in the semiclassical limit $\hbar \to 0$, the ϕ thus constructed is an asymptotic approximation to the exact solution, $\psi(q, t)$, of the time-dependent Schrödinger equation. In the special case where $\mathcal{C}_0$ is an invariant curve of the dynamics (e.g., if the Hamiltonian is time-independent and $\mathcal{C}_0$ is one of its contours) and where, moreover, θ represents an invariant measure on $\mathcal{C}_0$, then ϕ is an asymptotic approximation to a stationary state of the system.

What concerns us in the next two sections is the global breakdown of approximations of type (4) as $t \to \infty$ and $\mathcal{C}_t$ gets infinitely complicated. The point is that ϕ is valid as $\hbar \to 0$ for any fixed t, and not as $t \to \infty$ for any fixed $\hbar$, however small. We are not

concerned with isolated breakdowns of (4) at caustics (turning points), i.e., places, q^* (FIGURE 1), where $\mathcal{C}_t$ is perpendicular to the q axis so that two or more roots, $p_j(q)$, coalesce and ϕ diverges; near q^*, uniformly valid approximations to ψ can be constructed either by projection of Wigner's function[8] or by using an equation analogous to (4) for the semiclassical momentum wave function and then Fourier transforming to get ψ.[9-11] Nor are we concerned with the quantization of the area within closed curves $\mathcal{C}_0$ necessary to ensure that ϕ is single valued.[1]

Global breakdown of (4) occurs when $\mathcal{C}_t$ gets so complicated that most of its convolutions have areas h or smaller in phase space, or, alternatively, when most pairs of caustics q^* are separated on the q axis by less than a de Broglie wavelength.

QUANTIZING GENERIC AREA-PRESERVING MAPS OF THE PLANE

Consider the following discrete map of the classical phase plane:

$$\left.\begin{aligned} q_{n+1} &= q_n + p_n \\ p_{n+1} &= p_n - \frac{dV}{dq}(q_{n+1}) \end{aligned}\right\}. \tag{5}$$

This can be generated by the following time-dependent Hamiltonian acting over unit time:

$$\left.\begin{aligned} H(q,p,t) = p^2 \quad & (0 \le t < \tfrac{1}{2}) \\ 2V(q) \quad & (\tfrac{1}{2} \le t < 1) \end{aligned}\right\}. \tag{6}$$

Repeated action of the map corresponds to a system where, alternately, the force is switched off and the mass is made infinite. If V is more complicated than quadratic in q, then the map (5) exhibits generic behavior. This is illustrated in FIGURE 2, which shows the orbits of points for the case

$$V(q) = \frac{q^4}{4}. \tag{7}$$

The now-familiar hierarchy of elliptic and hyperbolic fixed points, smooth invariant curves, and chaotic areas is evident,[5,15] indicating that (5) is a good model for a section through the phase space of a generic higher-dimensional system.

FIGURE 3 shows the first five iterates $\mathcal{C}_n$ under (5) and (7) of the curve

$$\mathcal{C}_0 : \frac{p^2}{2} + \frac{q^4}{4} = \frac{1}{4}. \tag{8}$$

$\mathcal{C}_0$ lies almost entirely in the outer, hyperbolically escaping region of FIGURE 2. Its iterates get rapidly more complicated by throwing off tendrils[1,8] and increase in length as $\exp(\exp(3n))$ while preserving their area.

The main reason for studying the map (5) is that its Hamiltonian (6) can easily be quantized. Indeed, it is obvious that the time-evolution operator $\hat{U}$ taking states $|\psi_n\rangle$ at time n into states $|\psi_{n+1}\rangle$ at time $n + 1$ is

$$\hat{U} = \exp\left[\frac{-iV(\hat{q})}{\hbar}\right]\exp\left[\frac{-i\hat{p}^2}{2\hbar}\right]. \tag{9}$$

This means that, in the position representation, wave functions $\psi_n(q)$ iterate according to the integral equation

$$\psi_{n+1}(q) = (2\pi\hbar)^{-1/2}\exp\left[\frac{-i\pi}{4} - \frac{iV(q)}{\hbar}\right]\int_{-\infty}^{\infty} dq' \exp\left[\frac{i(q-q')^2}{2\hbar}\right]\psi_n(q'). \tag{10}$$

To see the quantum effects corresponding to the developing complication of FIGURE 3, the initial state $\psi_0(q)$ must be that associated with $\mathcal{C}_0$. According to (8), $\mathcal{C}_0$ is the contour $E = 1/4$ of the time-averaged Hamiltonian, $p^2/2 - q^4/4$, representing a particle in a quartic potential well; therefore, ψ_0 was taken to be an eigenstate of this Hamiltonian, with $\hbar$ chosen so that $E = 1/4$ was the energy of the 18th state; this value of $\hbar$ is shown as a square on the $n = 0$ qp plane in FIGURE 3.

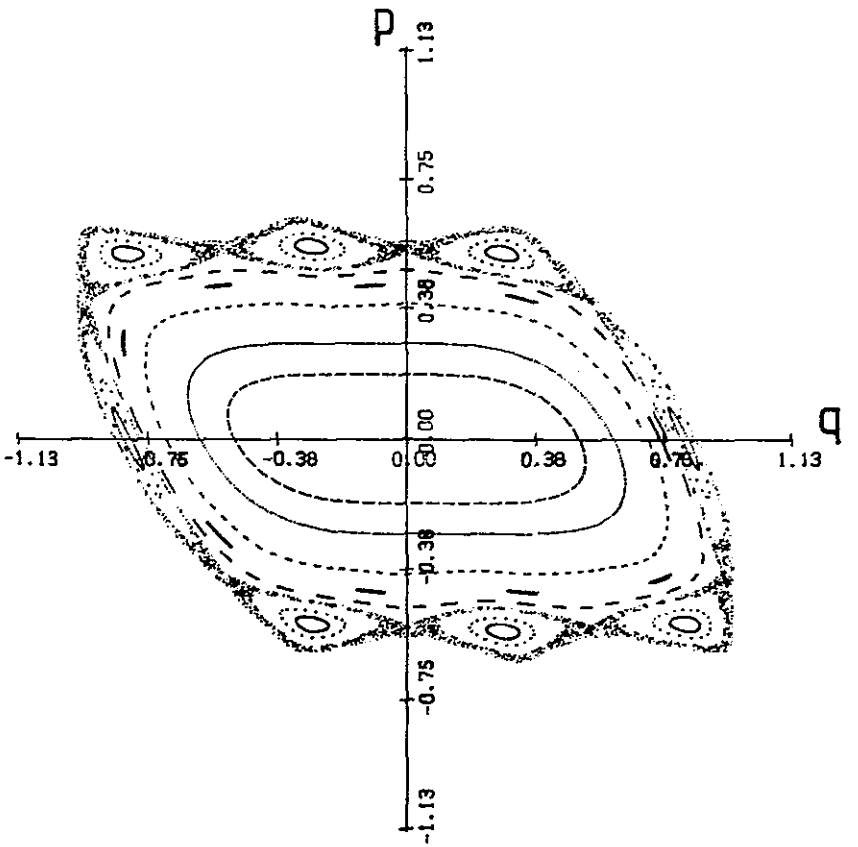

FIGURE 2. The orbits of points under the map given by equations 5 and 7, showing invariant curves and chaotic areas.

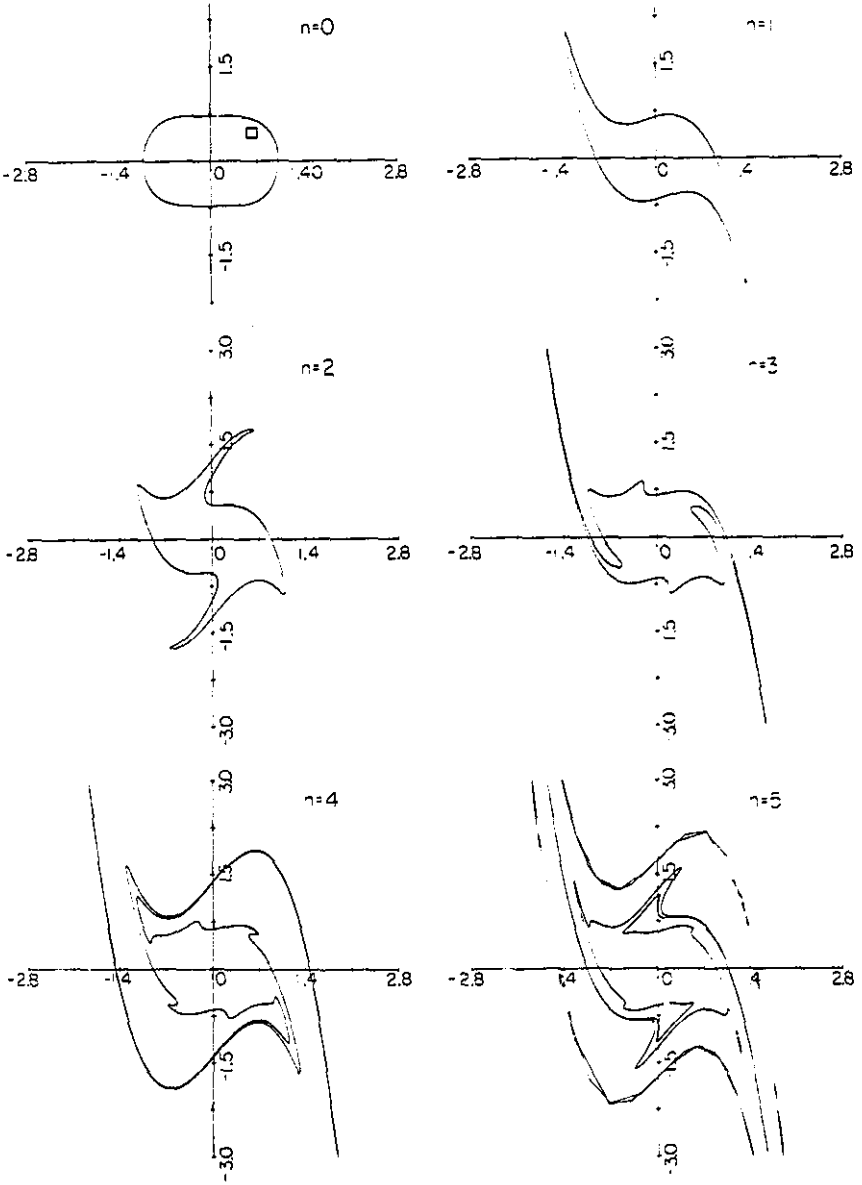

FIGURE 3. The evolution of curve $\mathcal{C}_0$ (8) for five iterations of the map of FIGURE 2, showing the development of tendrils.

The first five iterates of the probability density $|\psi_n(q)|^2$ are shown in FIGURE 4a. They should be compared with the curves $\mathcal{C}_n$ in FIGURE 3, and with the projections of these curves shown in FIGURE 5a. The singularities in FIGURE 5a are the caustics q^* (cf. FIGURE 1). For $n \leq 2$, the identification of classical and quantum features is fairly clear and shows that ψ_n and $\mathcal{C}_n$ are indeed associated as described in the previous section. Note the dramatic decrease in spectral purity of $\psi_2(q)$ as compared with $\psi_1(q)$; this is associated with the tendrils on $\mathcal{C}_2$, which cause a sudden increase in the number of branches $p_i(q)$ and, hence, in the contributions to the semiclassical wave function (4).

For $n > 2$, there is no clear association between ψ_n and individual features of $\mathcal{C}_n$. This represents a new regime of "quantum chaos." There is, however, on the average, an association between ψ_n and $\mathcal{C}_n$. This can be seen by smoothing $|\psi_n|^2$ and the curve projections over a de Broglie wavelength. The resulting quantum and classical smoothed curves are shown in FIGURES 4b and 5b, respectively. The correspondence is quite close and shows that, while the peaks of the smoothed $|\psi|^2$ for $n < 2$ are associated with individual caustics, the peaks for $n > 2$ are associated with clusters of caustics.

A greatly expanded account of the material in this section was published in Reference 1.

QUANTIZING A TWIST MAP

Tendrils growing on curves whose points map chaotically (as in FIGURE 3) do not represent the only way in which an evolving curve can get complicated. Even for regular motion (as in the central region of FIGURE 2), a curve that is not invariant will wrap around an elliptic fixed point and form a whorl as a result of its constituent points mapping round the fixed point at different rates.[1,8]

A simple model for classical and quantum whorls is provided by the time-independent Hamiltonian,

$$H(q,p) = f\left(\frac{(q^2 + p^2)}{2}\right), \tag{11}$$

where f is an arbitrary, smooth, nonlinear function of its argument. Classical motion is around circles centered on the origin, with radius $(p^2 + q^2)^{1/2}$ and action

$$I \equiv \oint \frac{p\mathrm{d}q}{2\pi} = \frac{(q^2 + p^2)}{2}. \tag{12}$$

The orbit with action I has the frequency

$$\omega(I) = \frac{\mathrm{d}H}{\mathrm{d}I} = \frac{\mathrm{d}f}{\mathrm{d}I}, \tag{13}$$

which varies with I because f is nonlinear. Therefore, radii map to spirals and (11) is a twist map.[5,16]

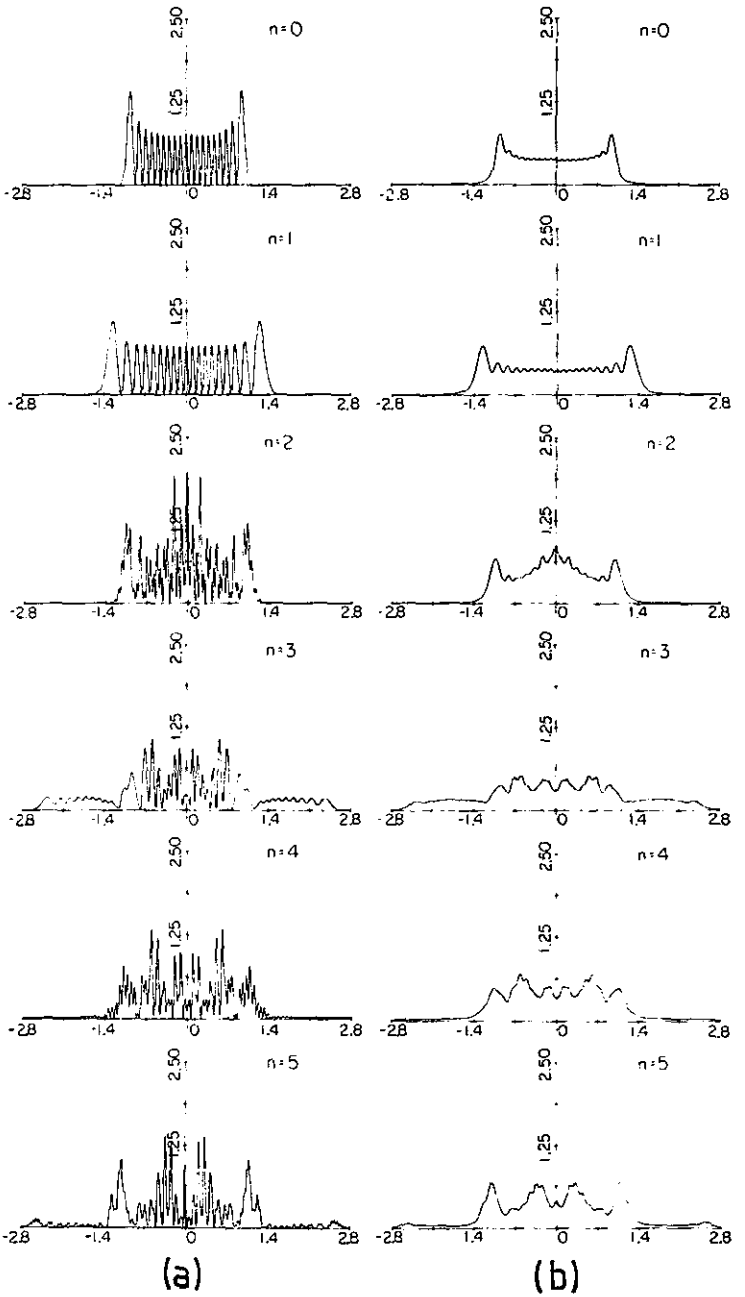

FIGURE 4. The evolution of (a) probability densities $|\psi_n|^2$ and (b) probability densities smoothed over a de Broglie wavelength, under the quantum map given by equation 10.

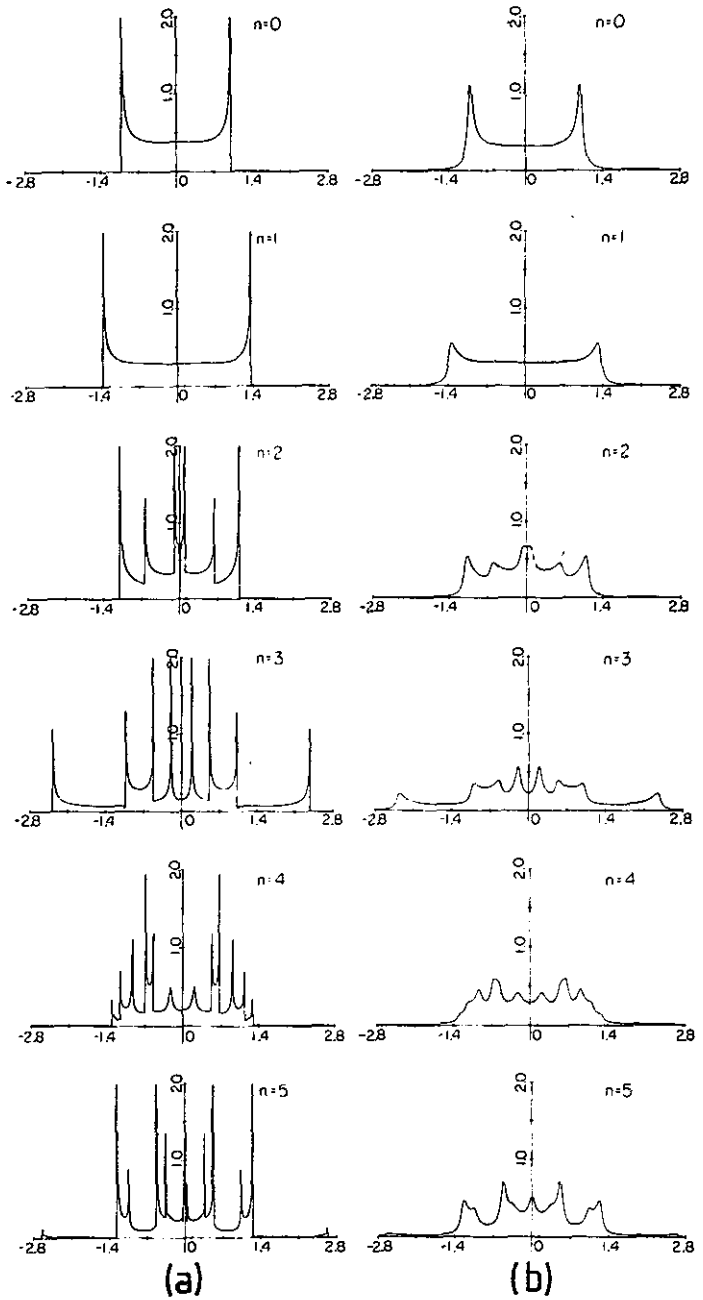

FIGURE 5. (a) Projections of curves of FIGURE 3, showing caustic spikes; (b) curves (a) smoothed over a de Broglie wavelength.

The quantum mechanics of this model is very simple, since H is a function of the harmonic oscillator Hamiltonian. Therefore, the energy levels are

$$E_n = f\left(\left(n + \frac{1}{2}\right)\hbar\right) \tag{14}$$

and the stationary states $\chi_n(q)$ are the familiar Hermite functions

$$\chi_n(q) = (2^n n!\hbar\sqrt{\pi})^{-1/2} H_n\left(\frac{q}{\hbar^{1/2}}\right)\exp\left[\frac{-q^2}{2\hbar}\right]. \tag{15}$$

Any initial state, $\psi(q, 0)$, can be expanded in terms of the χ_n so that the evolving state, $\psi(q, t)$, is given by

$$\psi(q, t) = \sum_{n=0}^{\infty}\left\{\int_{-\infty}^{\infty} dq'\psi(q', 0)\chi_n(q')\right\}\chi_n(q)\exp\left[-\frac{if}{\hbar}((n + \tfrac{1}{2})\hbar)t\right]. \tag{16}$$

Computations based on this model have been carried out by Z. V. Lewis, with the Hamiltonian function in (11) taken as $f(I) = \ln I$, for $t = 0$, 100π, 500π, and ∞. Classical curve maps $\mathcal{C}_t$ are shown on FIGURE 6a. $\mathcal{C}_0$ is a circle with radius $\sqrt{2 \times (30 + \frac{1}{2})} = 7.81$, whose center lies at $q = 1$, $p = 0$. The whorl develops very clearly as t increases. Its windings get tighter and tighter and, in the limit $t \to \infty$, the curve fills an annulus. FIGURE 6b shows the projections of $\mathcal{C}_t$ onto the q axis. Caustics proliferate, and, as $t \to \infty$, only their average density matters (in fact, this can be calculated analytically).

In the quantum mechanical computations, $\hbar$ was taken as untiy, so that $\mathcal{C}_0$ corresponded to an initial state

$$\psi(q, 0) = \chi_{30}(q - 1). \tag{17}$$

The evolving probability density $|\psi(q, t)|^2$ was calculated using (16). This equation shows that $\psi(q, t)$ continually changes, even as $t \to \infty$—behavior contrasting with that of $\mathcal{C}_t$, which tends to a limit, as shown in FIGURE 6a. Therefore, the association between $\mathcal{C}$ and ψ breaks down when t is large enough, as we shall see.

FIGURE 6d shows the probability densities. As t increases, ψ becomes spectrally richer, as would be expected from the increasing convolutions on FIGURE 6a. The curve $|\psi|^2$ for $t = \infty$ is actually a time average, which, from (16), is

$$\left|\psi(q, t)\right|^2_{\substack{\text{time}\\ \text{average}}} = \sum_{n=0}^{\infty}\left\{\int_{-\infty}^{\infty} dq'\psi(q', 0)\chi_n(q')\right\}^2\chi_n^2(q). \tag{18}$$

To facilitate comparison between the projections of $\mathcal{C}_t$ and the probability densities, both these sets of curves were smoothed over q by a de Broglie wavelength, as in the previous section; the smoothed classical curves are shown in FIGURE 6c and the smoothed quantal curves in FIGURE 6e. For $t = 0$ and $t = 100\pi$, the agreement is excellent and it is clear that the direct association between $\mathcal{C}$ and ψ holds accurately. But when $t = 500\pi$ there is no close relation between classical and quantal curves, even when smoothed. This is probably because the whorl's windings now have areas small in comparison with $\hbar$, so that their details are quantally irrelevant. Nevertheless, if the

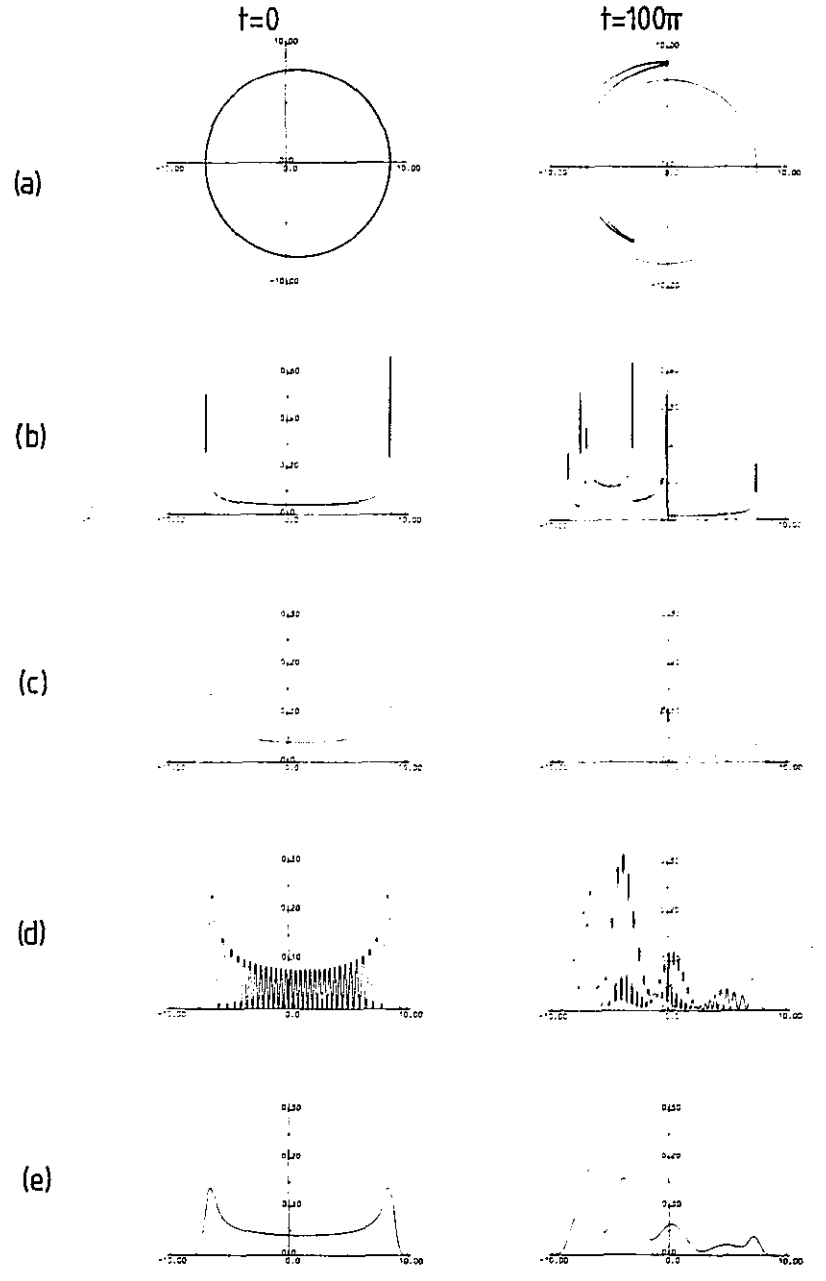

FIGURE 6. Classical and quantum maps based on the "nonlinear harmonic oscillator" Hamiltonian (11), with $f = \ln I$, for tim ' = 0, 100π, 500π, and ∞, computed by Z. V. Lewis. (a) Curves $\mathcal{C}$, evolving from initial curv ,, showing the development of a whorl; (b) projections of $\mathcal{C}$, showing caustic spikes;

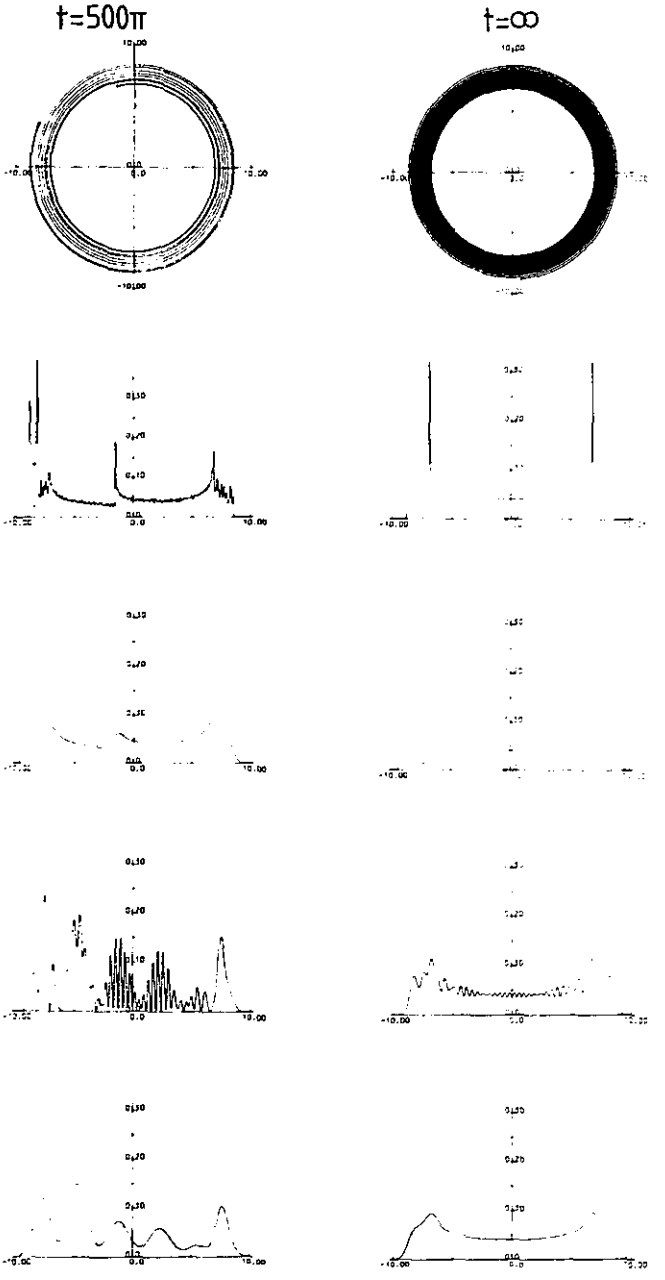

FIGURE 6. (*continued*) (c) smoothed projections of $\mathcal{C}_t$; (d) evolution of probability density $|\psi(q, t)|^2$, according to equation 16, starting from the initial wave (17) (for $t = \infty$, the time-average (18) is shown); (e) probability densities of (d) smoothed over a de Broglie wavelength.

quantum mechanical time average (18) is smoothed over q, the agreement with the smoothed projection of the fully developed whorl is very good, as the final pictures in FIGURE 6c and 6e show.

A full account of the material in this section will be published by Z. V. Lewis and M. V. Berry.

QUANTIZING ARNOL'D'S CAT

As a model for a completely ergodic system, consider the phase space to be the unit 2-torus $0 \le q \le 1$, $0 \le p \le 1$, with dynamics governed by the linear map

$$\begin{pmatrix} q_{n+1} \\ p_{n+1} \end{pmatrix} = T \begin{pmatrix} q_n \\ p_n \end{pmatrix}_{(\mathrm{mod}\ 1)} = \begin{pmatrix} T_{11} & T_{12} \\ T_{21} & T_{22} \end{pmatrix} \begin{pmatrix} q_n \\ p_n \end{pmatrix}_{(\mathrm{mod}\ 1)}. \tag{19}$$

The elements of T must be integers; this ensures that the map is continuous. The map is area-preserving if $\det T = 1$; this ensures that T can represent a Hamiltonian system. The map is hyperbolic if $|\mathrm{Tr}\, T| > 2$; together with the return of points to the torus, this ensures that shapes evolve chaotically under T. Maps of this type have become known by the collective title "Arnol'd's Cat."[7,15] An example is

$$T = \begin{pmatrix} 2 & 1 \\ 3 & 2 \end{pmatrix}, \tag{20}$$

which may be generated by the Hamiltonian

$$H = \frac{\operatorname{arcsinh} \sqrt{3}}{2} \left(\frac{p^2}{\sqrt{3}} - \sqrt{3}\, q^2 \right) \tag{21}$$

acting for unit time. This maps periodic figures into periodic figures in the qp plane while stretching them along asymptotes making an angle of 60° with the q axis.

Cat maps are interesting because, although their ergodicity indicates that they possess no invariant curves that could form the basis of Bohr-Sommerfeld semiclassical quantization, they can, nevertheless, be quantized exactly. The first aspect of quantization is purely kinematic. Because phase space is a unit torus, position wave functions $\psi(q)$ must have a unit period in q, implying that momentum wavefunctions $\bar{\psi}(p)$ must be series of delta functions at $p = nh$, where n is an integer and h is Planck's constant. But $\bar{\psi}(p)$ must also have a unit period in p. Taken together, these conditions imply that

$$h = \frac{1}{N}, \tag{22}$$

where N is an integer. This strange conclusion makes the model somewhat mechanically artificial, but its quantized form has a direct physical realization in optics in terms of diffraction by a periodic grating. Measurements of q or p can yield only values lying on the "quantum lattice,"

$$q = \frac{Q}{N}, \qquad p = \frac{P}{N} \qquad (1 \le Q, P \le N), \tag{23}$$

where Q and P are integers. In the classical limit, $N \to \infty$, q and p become continuous variables. For a technical reason that will not be explained here, N will henceforth be restricted to be odd.

The second aspect of quantization is the introduction of dynamics in the form of a unitary operator corresponding to T, analogous to equation 9 and propagating wave functions $\psi(Q)$, in the discrete representation (23) according to

$$\psi_{n+1}(Q) = \sum_{Q'=1}^{N} U_{QQ'}\psi_n(Q'). \tag{24}$$

This operator must preserve the periodicity in both q and p, a condition that can be shown to require that T have the form

$$T = \begin{pmatrix} \text{even} & \text{odd} \\ \text{odd} & \text{even} \end{pmatrix} \quad \text{or} \quad \begin{pmatrix} \text{odd} & \text{even} \\ \text{even} & \text{odd} \end{pmatrix} \tag{25}$$

(thus excluding the most familiar cat map, whose elements are 1, 1, 1, 2). The explicit construction of $U_{QQ'}$ for arbitrary maps of type (25) is an intricate process involving Gauss averaging and the Legendre and Jacobi sign symbols of number theory.[17] For the particular map (20), the evolution operator is

$$U_{QQ'} = \exp\left[\frac{-i\pi}{4}\right]\exp\left[\frac{2\pi i}{N}(Q^2 + Q'^2 - QQ')\right]\left(\frac{1}{\sqrt{N}}\right). \tag{26}$$

Eigenfunctions of the quantum map are states, $\psi(Q)$, that propagate into themselves under (24), apart from phase factors $\exp[i\alpha]$. These phase factors are the eigenfunctions of $\hat{U}$: they are defined by

$$\det(U_{QQ'} - \exp[i\alpha]\delta_{QQ'}) = 0. \tag{27}$$

This is an $N \times N$ determinant, so there are N "eigenangles" $\alpha_j (1 \le j \le N)$, and it is interesting to ask how these are distributed round the unit circle, especially in the classical limit, $N \to \infty$.

To answer this question, first consider the effect of a cat map on points in the quantum lattice (23). Being rational, these points map around closed orbits ("cycles"), in contrast to generic points on the torus, which have irrational coordinates and never return to their starting points. For each N, there will be a number $n(N)$ of iterations after which every rational point with denominator N will have completed at least one cycle. The number $n(N)$ is the period of the map; it is defined as the smallest number satisfying

$$T^{n(N)} = \begin{pmatrix} 1 & 0 \\ 0 & 1 \end{pmatrix}_{(\text{mod } N)}, \tag{28}$$

and given by the lowest common multiple of the lengths of the cycles of points in the quantum lattice. Now, for these linear maps whose Hamiltonians (e.g., (21)) are quadratic, certain quantum mechanical quantities (e.g., Wigner's function in phase space) evolve classically. It follows that, after $n(N)$ iterations of the quantum map, wave functions will have returned to themselves (apart from a possible phase factor), i.e.,

$$\hat{U}^{n(N)} = \hat{1} \exp [i\sigma(N)], \tag{29}$$

where σ is, in general, unknown. Therefore, the eigenangles must be multiples of $2\pi/n(N)$, apart from a shift, i.e.,

$$\alpha_i = \frac{2\pi m_i}{n(N)} + \frac{\sigma(N)}{n(N)} \qquad \begin{pmatrix} 1 \le j \le N \\ 1 \le m_i \le n(N) \end{pmatrix}. \tag{30}$$

The spectrum of $\hat{U}$ therefore consists of N eigenangles distributed among $n(N)$ possible eigenlevels. The number $n(N)$ is an extremely erratic function, defined number-theoretically by (28). Sometimes $n < N$, in which case some levels must be multiply occupied, and sometimes $n > N$, in which case some levels must be empty. In map (20), for instance,

$$n(1) = 1, \quad n(3) = 6, \quad n(5) = 3, \quad n(7) = 8, \quad n(9) = 18, \quad n(11) = 10. \tag{31}$$

Number-theoretical arguments, together with numerical experiments, strongly suggest that, in a suitably defined asymptotic sense,

$$n(N) \sim CN \quad \text{as} \quad N \to \infty, \tag{32}$$

where C is constant. But the limit is approached extremely slowly and erratically. Therefore, the semiclassical behavior of this chaotic system is very different from that of an integrable system, where the eigenvalues are smooth functions of h. In fact, decreasing h, and hence increasing N, causes the spectrum to depend on the iteration of points in an ever finer quantum lattice; the cycle structure thus revealed is increasingly complicated.

A greatly expanded account of the material in this section is being prepared for publication by J. H. Hannay and M. V. Berry.

Quantizing Sinai's Billiard

Consider a particle moving freely in the xy plane and being specularly reflected from circular discs of radius R whose centers are arrayed at the points of the unit square lattice (Figure 7a). R can vary between 0 and 0.5. This motion is equivalent to motion on a unit square with periodic boundary conditions with a central disc (Figure 7b), or to billiards on a torus with a hole (Figure 7c). This is one of the few systems with two degrees of freedom that is known to be ergodic;[18,19] as $t \to \infty$, almost every orbit passes almost every point of the square (Figure 7b) with almost every direction. The ergodicity is associated with hyperbolic instability, which derives from the continual defocusing of particle beams upon reflection at the disc. Alternatively, it is possible to think of each reflection as transferring the particle between two different sheets of the xy plane, so that the coordinate space is a sphere with two handles (Figure 7d) with infinite negative curvature concentrated on a circle;[18] ergodicity is then made plausible by the fact that motion on a manifold with constant negative curvature is ergodic.[18]

Because of its ergodicity, Sinai's Billiard is nonintegrable and cannot be quantized by the Bohr-Sommerfeld rules. But, because of its periodicity, the system can be

quantized using methods developed for the quantum mechanics of electrons in solids.[20] The wave equation is

$$\frac{\partial^2\psi}{\partial x^2} + \frac{\partial^2\psi}{\partial y^2} + (2\pi)^2 E\psi = 0, \tag{33}$$

and this must be solved subject to the conditions that ψ vanishes on the boundaries of the discs in FIGURE 7a and that ψ has the periodicity of the lattice: these conditions determine the energy eigenvalues E (the factor $(2\pi)^2$ is chosen purely for convenience).

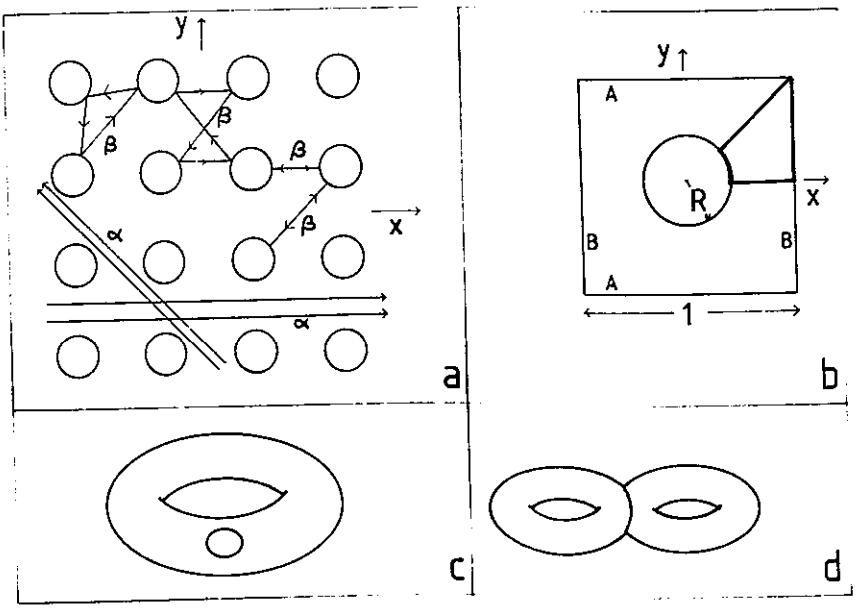

FIGURE 7. Representations of Sinai's Billiard. (a) As a regular array of reflecting discs, showing orbits (α) that never hit a disc, and closed orbits (β) that do hit a disc; (b) as a square with opposite edges identified, containing a hard disc; (c) as a torus with a reflecting hole; (d) as a sphere with two handles, consisting of two tori joined on a circle on which the Gaussian curvature is infinitely negative.

By expanding ψ in angular eigenfunctions and using a two-dimensional version[21] of the Korringa-Kohn-Rostoker (KKR) method of electron band theory,[20] it is found that the energies satisfy

$$\det_{ll'}[\delta_{ll'} + \tan\eta_l(E) S_{l-l'}(E)] = 0 \qquad (-\infty < (l, l') < \infty). \tag{34}$$

The η_l are the scattering phase shifts, which for a disc are

$$\tan\eta_l(E) = \frac{J_l(2\pi R\sqrt{E})}{Y_l(2\pi R\sqrt{E})}, \tag{35}$$

where J and Y denote the usual Bessel functions. The S_l are the KKR structure constants; they are defined by

$$S_l(E) = \sum_{\mathbf{r}}' Y_l(2\pi r\sqrt{E}) \exp[il\theta_r], \tag{36}$$

where the summation is over vectors $\mathbf{r}$ of the unit lattice, excluding $\mathbf{r} = 0$, and θ_r is the angle made by $\mathbf{r}$ with the x axis. In physical terms, the determinantal equation (34) is the condition for constructive interference of waves scattered from the disc at $\mathbf{r} = 0$ with waves reaching the neighborhood of that disc after multiple scattering from and amongst the other discs.

The symmetry of the system (FIGURE 7b) gives rise to degeneracies, for example, between wave functions related by reflection in a diagonal of the square. Such degeneracies can be eliminated by considering only those states which are antisymmetric about $x = 0$ and $x = y$, so that the problem becomes one of determining the vibrations of a membrane clamped at its boundary, which has the form of the heavy line in FIGURE 7b. For this subclass of quantum billiard states, the energies are given by the following equation, derived from (34):

$$\det_{n,n'}[\delta_{nn'} + \tan \eta_{4n}(E)\{S_{4(n-n')}(E) - S_{4(n+n')}(E)\}] = 0 \qquad (1 \le (n, n') < \infty). \tag{37}$$

Of all band structure methods, KKR gives the most compact representation. More conventional methods would involve expanding ψ in a basis set of states labeled by two indices, leading to determinants in which, in contrast to (34) and (37), each element is labeled by four indices. Moreover, the rapid decrease in $\tan \eta_l$ when $l > 2\pi R\sqrt{E}$ gives

TABLE 1

ENERGY LEVELS E_n FOR DIFFERENT VALUES OF R

	R				
n	0.0	0.1	0.2	0.3	0.4
1	5.00	5.00	5.17	6.53	11.78
2	10.00	10.01	10.82	12.67	20.27
3	13.00	13.03	13.92	18.24	28.05
4	17.00	17.07	18.21	22.07	33.87
5	20.00	20.16	23.52	27.78	40.38
6	25.00	25.08	25.71	31.14	47.34
7	26.00	26.17	27.93	36.87	57.40
8	29.00	29.46	34.08	41.57	59.60
9	34.00	34.41	37.66	42.91	68.51
10	37.00	37.26	40.95	50.68	74.74
11	40.00	40.60	41.79	53.58	77.83
12	41.00	41.37	46.86	58.53	89.91
13	45.00	46.08	51.02	60.92	91.43
14	50.00	50.27	55.22	66.98	98.87
15	52.00	52.31	57.12	69.36	105.52
16	53.00	54.50	61.76	72.85	109.63
17	58.00	59.76	63.07	79.86	114.72
18	61.00	61.38	66.44	84.21	121.05
19	65.00	65.02	72.07	87.93	131.23
20	65.00	66.40	72.72	89.29	132.24

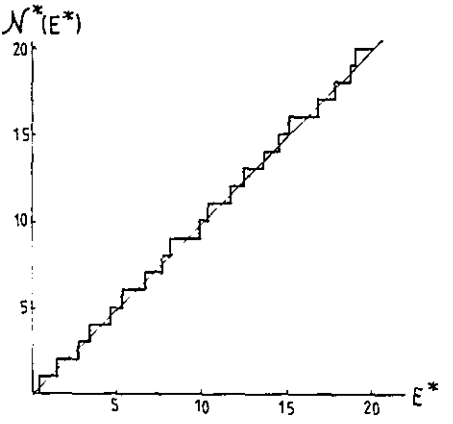

FIGURE 8. Energy levels of the quantum Sinai billiard for $R = 0.3$ plotted as a function of the variable E^* (41), for which the average density of states is unity. $\mathcal{N}^*(E^*)$ is the number of levels n for which $E_n^* < E^*$ (42).

very rapid convergence. In the case of (37), the Nth energy level can be computed to high accuracy with the determinant truncated at $n = n' = n_{max}$, where

$$n_{max} = R\left(\frac{2\pi N}{(1 - \pi R^2)}\right)^{1/2}. \tag{38}$$

If $R = 0.4$, for example, the first 100 levels can be computed from a 15×15 determinant. The series (36) for the structure constants converges very slowly, but can be transformed by a (nontrivial) application of the Ewald summation procedure into an exponentially convergent representation.

In the "unperturbed" limit $R = 0$, the levels are integers given by

$$E = m^2 + n^2 \qquad (1 \leq m < n < \infty). \tag{39}$$

Although symmetry degeneracies (e.g., m, n and n, m, or m, n and m, $-n$) have been eliminated, number-theoretic degeneracies remain; the first is at $E = 65 = 8^2 + 1^2 = 7^2 + 4^2$. The average density of states in E is $\pi/8$.[22] These states are very irregularly distributed as $E \to \infty$ because the probability that any integer E can be expressed as the sum of two squares decreases like $(\ln E)^{-1/2}$ as $E \to \infty$.[22] Therefore, the asymptotic (semiclassical) spectrum for $R = 0$ consists of increasingly large gaps between levels with increasing degeneracy.

Energy levels were computed for $R > 0$ using (37). The lowest twenty levels, for $R = 0$ to 0.4 in steps of 0.1, are listed in TABLE 1. It is possible to compare these results with theoretical predictions in several ways. Consider first the mode number (integrated density of states function) $\mathcal{N}(E)$, defined as

$$\mathcal{N}(E) = \text{number of states with } E_n < E = \sum_{n=1}^{\infty} \Theta(E - E_n), \tag{40}$$

where E_n labels the energy states and Θ denotes the unit step function. It is known that, for a membrane such as that outlined in FIGURE 7b, $\mathcal{N}(E)$, suitably smoothed, possesses an asymptotic expansion in decreasing powers of E, whose successive terms depend on the area of the membrane, and the length, corner angles, and curvatures of its boundary.[23] When applied to the present problem, the expansion gives

$$\mathcal{N}(E) \sim E^*(E) \approx \frac{\pi}{8}(1 - \pi R^2)E - \frac{1}{2}\left(1 + 2^{-1/2} - R\left(2 - \frac{\pi}{4}\right)\right)E^{1/2} - \frac{31}{96}. \quad (41)$$

For comparison with the numerical computations, it is sensible to plot

$$\mathcal{N}^*(E^*) \equiv \sum_{n=1}^{\infty} \Theta(E^* - E^*(E_n)) \quad (42)$$

rather than $\mathcal{N}(E)$, and such a graph is shown in FIGURE 8 for the (typical) case $R = 0.3$. Agreement with the theoretical 45° straight line is very good. If only the leading "Weyl" term in (41) is retained, then the agreement is poor.

It is exceptional for the eigenvalues of a vibrating system to be degenerate, even if a single parameter is varied[18] (in general, a degeneracy is achieved by varying two parameters). Therefore, no degeneracies except those at $R = 0$ (which arise from the special, integrable nature of the unperturbed system) are expected in the quantum Sinai Billiard. And, indeed, none have been found, despite an extensive search. Quite frequently, two levels approach one another as R varies, but they always repel rather than cross. Several examples of this behavior are shown in FIGURE 9.

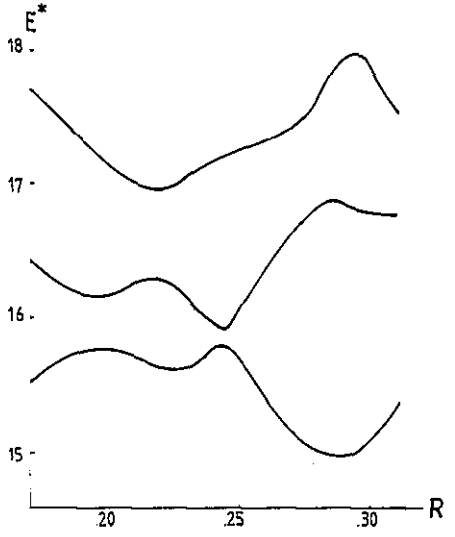

FIGURE 9. Some energy levels of the quantum Sinai Billiard as a function of R, showing near degeneracies.

Finally, it is possible to expand the KKR determinant (34) by analytical means and study the effect of closed orbits on the spectrum embodied in the density of states function

$$n(E) = \frac{d\mathcal{N}(E)}{dE} = \sum_{n=1}^{\infty} \delta(E - E_n). \quad (43)$$

Lack of space prevents more than a summary of the instructive results of this analysis. The expansion employed is different from the usual multiple-scattering series of KKR

theory,[20] and leads to three different types of contributions to $n(E)$:

1. A constant term, analogous to the leading term in (41) and giving the average density of states.

2. Oscillatory terms, proportional to $E^{-1/4}$, from each topologically distinct closed classical orbit that never strikes a disc, e.g., those labeled α in FIGURE 7a. Such orbits are not isolated; they occur in families resembling the closed orbits of an integrable system[24] and, indeed, contribute similarly to $n(E)$.

3. Oscillatory terms, proportional to $E^{-1/2}$, from each topologically distinct closed classical orbit that does strike a disc, e.g., those labeled β in FIGURE 7a. All such orbits are isolated and unstable, and their contributions to $n(E)$ are in precise agreement with the predictions of earlier, more general studies of the effect of unstable closed orbits.[25-27]

The resulting semiclassical expansion of $n(E)$ for the full spectrum (i.e., that including states of all symmetry types), complete for terms of types 1 and 2 and including the simplest terms of type 3, namely those corresponding to bounces between pairs of discs, is as follows:

$$n(E) \simeq \pi(1 - \pi R^2) + E^{-1/4} \sum_{\mathbf{r}}{}' \frac{(1 - 2Rr)\Theta(1 - 2Rr)}{r^{1/2}} \sum_{m=1}^{\infty} \frac{\cos\left[2\pi m r\sqrt{E} - \frac{\pi}{4}\right]}{m^{1/2}}$$

$$+ E^{-1/2} \sum_{\mathbf{r}}{}' (r - 2R)\Theta(1 - Rr)$$

$$\times \sum_{m=1}^{\infty} \frac{\cos\left[4\pi m(r - 2R)\sqrt{E}\right]}{\left\{\sqrt{\frac{r}{2R}} + \sqrt{\frac{r}{2R} - 1}\right\}^{2m} - \left\{\sqrt{\frac{r}{2R}} + \sqrt{\frac{r}{2R} - 1}\right\}^{-2m}} + \cdots \qquad (44)$$

In this formula, $\mathbf{r} \equiv (p, q)$, where p and q are relatively prime integers (positive and negative) not both zero, $r \equiv \sqrt{(p^2 + q^2)}$, and $\cdots$ denotes the contribution from unstable closed orbits involving three or more discs.

Although their contributions are individually weaker, unstable closed orbits are much more numerous than nonisolated orbits, and must eventually dominate the spectrum by interfering to form the delta functions in (43), in a manner not understood at present. It is, therefore, interesting to try to discern the effect of the unstable orbits on the small number of energy levels so far calculated. One such effect is in the R-dependence, rather than the E-dependence, of $n(E)$. According to (44), only the unstable orbits have oscillatory R-dependence, suggesting that levels with energy near E should vary with R, with a "wavelength"

$$\Delta R = (4\sqrt{E})^{-1}. \qquad (45)$$

This is in rough agreement with the R-variation in FIGURE 9, for which $\Delta R \sim 0.03$.

The material in this section, which will soon be published in greatly expanded form, complements a recent pioneering computational study of another completely ergodic system, namely the stadium (which consists of billiards in an enclosure consisting of two semicircular arcs joined by tangential straight lines).[12]

REFERENCES

1. BERRY, M. V., N. L. BALAZS, M. TABOR & A. VOROS. 1979. Ann. Phys. (N. Y.) **122:** 26–63.
2. POMPHREY, N. 1974. J. Phys. B **7:** 1909–15.
3. NOID, D. W. & R. A. MARCUS. 1975. J. Chem. Phys. **62:** 2119–24.
4. STRATT, R. M., N. C. HANDY & W. H. MILLER. 1979. J. Chem. Phys. **71:** 3311–22.
5. BERRY, M. V. 1978. *In* Topics in Nonlinear Mechanics. S. Jorna, Ed. Am. Inst. Phys. Conf. Proc. **46:** 16–120.
6. PERCIVAL, I. C. 1977. Adv. Chem. Phys. **36:** 1–61.
7. ARNOL'D, V. I. & A. AVEZ. 1968. Ergodic Problems of Classical Mechanics. Benjamin. New York.
8. BERRY, M. V. & N. L. BALAZS. 1979. J. Phys. A **12:** 625–42.
9. KRAVTSOV, YU. A. 1968. Sov. Phys. Acoust. **14:** 1–17.
10. MASLOV, V. P. 1972. Theorie des Perturbation et des Methodes Asymptotiques. Dunod. Paris.
11. BERRY, M. V. & F. J. WRIGHT. 1980. J. Phys. A **13:** 149–60.
12. MCDONALD, S. W. & A. N. KAUFMAN. 1979. Phys. Rev. Lett. **42:** 1189–91.
13. UHLENBECK, K. 1976. Am. J. Math. **98:** 1059–78.
14. PERCIVAL, I. C. 1973. J. Phys, B **6:** L229–32.
15. FORD, J. 1975. *In* Fundamental Problems in Statistical Mechanics III. M. Cohen, Ed.: 215–55. North-Holland. Amsterdam.
16. MOSER, J. 1962. Nachr. Akad. Wiss. Göttingen Math Phys. Kl 2A: Math.-Phys.-Chem. Abt. **1:** 1–20.
17. RADEMACHER, H. 1964. Lectures on Elementary Number Theory. Blaisdell. New York.
18. ARNOL'D, V. I. 1978. Mathematical Methods of Classical Mechanics. Springer-Verlag. New York.
19. SINAI, YA. G. 1970. Russ. Math. Surv. **25** (2): 137–87.
20. ZIMAN, J. M. 1971. Solid State Phys. **26:** 1–101.
21. OZORIO DE ALMEIDA, A. M. 1975. Acta. Crystallogr. Sect. A **31:** 435–42, 442–45.
22. SIERPINSKI, W. 1964. Elementary Theory of Numbers. Pol. Acad. Mon. Math., Vol. 42. Warsaw.
23. BALTES, H. P. & E. R. HILF. 1976. Spectra of Finite Systems. B-I. Wiss. Mannheim.
24. BERRY, M. V. & M. TABOR. 1976. Proc. R. Soc. London Ser. A **349:** 101–23. 1977. J. Phys. A **10:** 371–79.
25. GUTZWILLER, M. C. 1971. J. Math. Phys. **12:** 343 58.
26. GUTZWILLER, M. C. 1978. *In* Path Integrals and Their Applications in Quantum, Statistical and Solid State Physics. G. J. Papadopoulos and J. T. Devreese, Eds.: 163–200. Plenum. New York.
27. BALIAN, R. & C. BLOCH. 1972. Ann. Phys. (N.Y.) **69:** 76–160.